Supporting information: Delving into Theoretical and Computational Considerations for Accurate Calculation of Chemical Shifts in Paramagnetic Transition Metal Systems using quantum chemical methods

Md. Ashraful Islam*, and Andrew J. Pell*

CRMN Lyon, ENS de Lyon

E-mail: ashraful.islam@ens-lyon.fr,andrew.pell@ens-lyon.fr

The metal-nuclear hyperfine tensor In the non-relativistic theory with spin-orbit coupling (SOC) described as perturbation, the hyperfine coupling can be separated into the anisotropic dipolar and isotropic Fermi contact contributions. These two contributions to the hyperfine coupling are calculated using the following equations,

$$A_{Kij}^{dip} = \frac{\mu_0 \mu_B}{4\pi} \gamma_K \hbar g_e \left[\sum \rho_{pq}^{\alpha-\beta} \left\langle \phi_p \left| \hat{T}_{Kij} \right| \phi_q \right\rangle - \frac{1}{N} \sum_{kl} \frac{\partial \rho_{pq}^{\alpha-\beta}}{\partial I_{Ki}} \left\langle \phi_p \left| \hat{h}_j^{SOC} \right| \phi_q \right\rangle \right] \tag{S1}$$

$$A_K^{FC} = \frac{2}{3} \mu_0 \mu_B g_e \gamma_K \hbar \left\langle S_z \right\rangle^{-1} \sum \rho_{pq}^{\alpha-\beta} \delta \left(\mathbf{r} - \mathbf{r_K} \right) \tag{S2}$$

where g_e is the free-electron g-factor, μ_0 is the magnetic permeability, μ_B is the Bohr magneton, $\rho^{\alpha-\beta}$ is the spin density matrix in the molecular orbital basis $\{\phi\}$, I_K and γ_K are the spin quantum number and gyromagnetic ratio of nucleus K, respectively. $\hat{h}_j^{SOC}$ is the effective one-electron SOC Hamiltonian which includes the effect of SOC in the hyperfine

tensors, and $\hat{T}_{Kij} = r^{-5}\left(3\hat{r}_{Ki}\hat{r}_{Kj} - r_K^2\delta_{ij}\right)$ where $\mathbf{r}_K$ is the distance from metal to nucleus K. Eq. S1 is solved through coupled perturbed SCF iterative technique with respect to the nucleus-electron orbit coupling as (coupled) perturbation. The first and last terms of eq. S1 separates the spin-dipolar A_{Kij}^{SD} and orbital A_{Kij}^{Orb} contributions of the unpaired electrons to the dipolar hyperfine tensor.

It is essential to recognize that the discussion on hyperfine interaction here pertains to a classical non-relativistic standpoint. In both the minimally coupled four-component relativistic Dirac theory and non-relativistic Lévy-Leblond theory for electrons, there is an absence of a term involving a delta function as given in eq. S2. Consequently, the concept of a contact interaction does not arise within these frameworks. Instead, the first-order interaction terms in the two-component theory, which are derived from either the four-component Dirac equation or the Lévy-Leblond equation, naturally give rise to the contact interaction[1]. Moreover, the mathematical forms of hyperfine operators in the two-component methods can vary depending on how the four-component Dirac theory is reduced to the two-component method. The phenomenon known as "picture change effects" associated with the hyperfine interaction is discussed in references such as[2–7] for the two-component approaches like ZORA, DKH, X2C. Relativistic effects are generally minimal in the context of light atoms and thus for the sake of brevity we have discussed focusing on the non-relativistic level of theory.

The point-dipole approximation of the hyperfine tensor In the point dipole approximation, the dipolar contributions of the hyperfine tensor reduces to

$$\begin{aligned} A_{Kij}^{dip} &= \frac{\mu_0\mu_B}{4\pi}\gamma_K\hbar\sum_{ijk} g_{ik}T_{kj} \\ &= \frac{\mu_0\mu_B}{4\pi}\gamma_K\hbar g_e\sum_{ij} T_{ij} + \frac{\mu_0\mu_B}{4\pi}\gamma_K\hbar\sum_{ikj}\Delta g_{ik}T_{kj} \end{aligned} \tag{S3}$$

Hence, considering the form of the hyperfine tensor of eq. S3 leads to the evaluation of

the dipolar hyperfine shielding according to eq. 1 in a semi-classical fashion,

$$\sigma^{p}_{Kij} = -\frac{1}{4\pi N_A}\sum_{ij}\chi_{ik}\cdot T_{kj} \tag{S4}$$

which can be separated into the pure spin-dipolar (SD) and orbital (PSO) contrbutions,

$$\sigma^{SD}_{Kij} = -\frac{1}{4\pi N_A}\sum_{ij}\chi^{s}_{ik}\cdot T_{kj} \tag{S5}$$

$$\sigma^{PSO}_{Kij} = -\frac{1}{4\pi N_A}\sum_{ij}\chi^{s}_{ik}\cdot \Delta g_{kl}\cdot T_{Klj}$$

by considering the shifts of the g-tensor component from the free electron value, $g_{ik} = g_e - \Delta g_{ik}$. Note that, the χ_{ik} in eq. S4 is the component of the Van Vleck paramagnetic susceptibility whereas in eq. S5 χ^{s}_{ik} is the spin-only component to the Van Vleck paramagnetic susceptibility.

Table S1: SO energy levels (in cm^{-1}) due to the state interactions of the two energetically lowest SF states from CAS based methods. The SO energy levels are doubly degenerate.

	$CoTp_2$		$[Co(AcPyOx)_3(BPh)]^+$	
n°	SF-CASSCF	SF-CASPT2	SF-CASSCF	SF-CASPT2
1	0	0	0	0
2	34	44	386	499
	SO-CASSCF	SO-CASPT2	SO-CASSCF	SO-CASPT2
1	0	0	0	0
2	276	268	270	246
3	554	541	775	839
4	830	809	1046	1086

Table S2: SO energy levels (in cm^{-1}) due to the state interactions of all the quintet and doublet SF states from CAS based methods. The SF energy states of the ground ^4F manifolds are given. The SO energy levels are doubly degenerate.

	$CoTp_2$		$[Co(AcPyOx)_3(BC_6H_5)]^+$	
n°	SF-CASSCF	SF-CASPT2	SF-CASSCF	SF-CASPT2
1	0	0	0	0
2	34	44	386	499
3	1820	2316	4723	5723
4	8185	9586	7276	8703
5	8408	9710	7569	9045
6	8946	10005	8235	9481
7	17631	21974	13277	16211
	SO-CASSCF	SO-CASPT2	SO-CASSCF	SO-CASPT2
1	0	0	0	0
2	241	232	230	209
3	514	501	729	796
4	843	811	1030	1069
5	2242	2689	4934	5896
6	2335	2785	5035	5991
7	8581	9923	7548	8930

Table S3: SF and SO CAS based energy levels (in cm^{-1}) calculated from ORCA 5.0 to verify the effects of NEVPT2 dynamical correlation correction with the CASPT2 results from Table S2. The SF energy states of the ground ^4F manifolds are given. The SO energy levels are doubly degenerate. The computational details is similar to the hyperfine calculation from CAS space in ORCA as mentioned in the main text except TZVP basis set was utilized for the ligand atoms.

	$CoTp_2$		$[Co(AcPyOx)_3(BC_6H_5)]^+$	
n°	SF-CASSCF	SF-NEVPT2	SF-CASSCF	SF-NEVPT2
1	0	0	0	0
2	33	42	380	507
3	1881	2431	4718	6024
4	8125	10658	7269	9707
5	8353	10969	7564	10128
6	8928	11780	8208	11036
7	17513	22475	13221	16937
	SO-CASSCF	SO-NEVPT2	SO-CASSCF	SO-NEVPT2
1	0	0	0	0
2	235	235	224	205
3	501	504	713	797
4	819	810	1004	1058
5	2288	2813	4924	6209
6	2376	2895	5020	6292
7	8510	9786	7532	9933

Table S4: The SO-CAS based EPR spin Hamiltonian parameters of the two lowest KDs modeled with a pseudospin $\tilde{S} = 3/2$.

		$g_\perp$	$g_\parallel$	D	E
$CoTp_2$	SO-CASSCF	1.74,1.79	3.27	-114.7	21.1
	SO-CASPT2	1.72,1.76	3.25	-112.4	15.8
	Exp[a]	1.9	2.1	-98.5[a]	
$[Co(AcPyOx)_3(BPh)]^+$	SO-CASSCF	1.95,1.98	3.25	-114.8	3.2
	SO-CASPT2	1.96,2.00	3.16	-104.4	2.4
	Exp[b]	2.08	3.09	-86	
	[c]	2.22	2.86	-95	

[a]:from the fit of THz-EPR spectra[8], [b]: from the fit of SQUID magnetic susceptibility, [c] : from the fit of $\Delta\chi_{ax}$ determined from paramagnetic NMR shifts[9].

Table S5: Experimentally reported chemical shifts (in ppm) in the $[M(AcPyOx)_3(BPh)]^+$ complexes from Ref.[9]. The paramagnetic chemical shifts (Para) (in ppm) in the paramagnetic Mn(II), Ni(II) and Co(II) complexes are evaluated with respect to the diamagnetic Fe(II) complex.

	Fe	Mn	Ni	Co	Para		
					Mn	Ni	Co
o-PhC	131.7	145.4	147.7	208.6	13.7	16.0	76.9
m-PhC	127.4	131.3	130.0	164.7	3.9	2.6	37.3
p-PhC	128.0	127.9	128.0	155.4	-0.1	0.0	27.4
i-PhC	-	-	78.4	-	-	-	-
o′-PyC	153.0	-	-9.6	263.9	-	-162.6	110.9
m′-PyC	125.8	635.9	544.2	554.9	510.1	418.4	429.1
p-PyC	137.9	391.6	116.3	146.7	253.7	-21.6	8.8
m″-PyC	124.5	188.2	393.1	318.3	63.7	268.6	193.8
o″-PyC	158.0	-	-116.9	-476.5	-	-274.9	-634.5
*C=N	160.6	807.0	54.0	97.7	646.4	-106.6	-62.9
*CH3	13.2	11.7	322.0	189.4	-1.5	308.8	176.2
o-PhH	7.8	8.5	7.4	67.9	0.7	-0.4	60.1
m-PhH	7.4	7.3	6.6	29.9	-0.1	-0.8	22.5
p-PhH	7.4	7.5	6.9	25.7	0.1	-0.5	18.3
o′-PyH	7.1	104	137.3	396.2	96.9	130.2	389.1
m′-PyH	7.5	47.0	44.1	80.1	39.5	36.6	72.6
p-PyH	8.1	-25.9	15.5	15.1	-34.0	7.4	7.0
m″-PyH	7.9	47.0	59.9	-2.5	39.1	52.0	-10.4
CH3*	2.7	-	-24.0	2.4	-	-26.7	-0.3

Table S6: The SD and PSO contributions (in ppm) of the dipolar hyperfine tensors to the dipolar chemical shifts (Dip) in the $[Ni(AcPyOx)_3(BPh)]^+$ complex. The dipolar hyperfine tensors are evaluated according to the two QC methods, namely the unrestricted DFT ZORA-PBE0 and SO-CASSCF, for comparison.

	ZORA-PBE0			SO-CASSCF		
	SD	PSO	Dip	SD	PSO	Dip
o-PhC	-1.0	0.0	-1.0	-0.9	-1.0	-1.9
m-PhC	-0.5	-0.1	-0.6	-0.5	-0.5	-1.0
p-PhC	-0.4	-0.1	-0.5	-0.4	-0.4	-0.8
i-PhC	-1.6	0.2	-1.4	-1.6	-1.5	-3.1
o′-PyC	-3.1	7.8	4.7	-2.1	1.0	-1.1
m′-PyC	-0.4	-0.9	-1.3	-0.4	0.3	-0.1
p-PyC	-0.2	0.5	0.3	0.2	0.6	0.8
m″-PyC	0.9	1.1	2.0	0.8	1.1	1.9
o″-PyC	1.6	3.5	5.1	2.6	2.9	5.5
*C=N	-1.1	8.1	7.0	2.2	2.3	4.5
*CH3	0.6	1.9	2.5	0.6	0.5	1.1
o-PhH	0.0	0.0	0.0	-0.8	-0.9	-1.7
m-PhH	0.0	0.0	0.0	-0.3	-0.4	-0.7
p-PhH	0.0	0.0	0.0	-0.3	-0.3	-0.6
o′-PyH	-0.1	-0.4	-0.5	-2.9	-1.5	-4.4
m′-PyH	0.0	0.0	0.0	-0.4	0.0	-0.4
p-PyH	0.0	0.2	0.2	0.1	0.2	0.3
m″-PyH	0.0	0.6	0.6	0.6	0.5	1.1
CH3*	0.0	0.2	0.2	0.3	0.0	0.3

Table S7: Experimental and calculated chemical shifts (in ppm) in the $[Ni(AcPyOx)_3(BPh)]^+$ complex according to the VV, mPV and BB approaches. The orbital (Orb) contributions (in ppm) to the calculated shifts were evaluated from the ZORA-PBE0 method and the paramagnetic contributions (Para) (in ppm) were evaluated according to eq. 1 where the A_K tensors are from the ZORA-PBE0 method while the χ^s tensors were evaluated according to the three approaches from SO-CASPT2 results.

	Exp	Cal			Orb	Para		
		VV	mPV	BB		VV	mPV	BB
o-PhC	147.7	149.0	148.9	149.1	139.7	9.3	9.2	9.4
m-PhC	130	138.4	138.4	138.4	136.3	2.1	2.1	2.1
p-PhC	128	136.9	136.9	136.9	138.0	-1.1	-1.1	-1.1
i-PhC	78.4	86.2	86.5	85.9	147.0	-60.8	-60.5	-61.1
o′-PyC	-9.6	-47.6	-46.7	-48.7	156.5	-204.1	-203.2	-205.2
m′-PyC	544.2	594.1	592.1	596.6	132.4	461.7	459.7	464.2
p-PyC	116.3	130.0	130.1	129.9	150.9	-20.9	-20.8	-21.0
m″-PyC	393.1	418.7	417.5	420.3	132.0	286.7	285.5	288.3
o″-PyC	-116.9	-71.7	-70.7	-73.0	164.7	-236.4	-235.4	-237.7
*C=N	54	53.8	54.2	53.2	163.0	-109.2	-108.8	-109.8
*CH3	322	396.2	394.5	398.3	12.0	384.2	382.5	386.3
o-PhH	7.4	8.2	8.2	8.2	7.9	0.3	0.3	0.3
m-PhH	6.6	7.0	7.0	7.0	7.7	-0.7	-0.7	-0.7
p-PhH	6.9	7.6	7.6	7.6	7.7	-0.1	-0.1	-0.1
o′-PyH	137.3	155.8	155.1	156.6	7.9	147.9	147.2	148.7
m′-PyH	44.1	45.0	44.8	45.2	7.6	37.4	37.2	37.6
p-PyH	15.5	17.3	17.2	17.3	8.4	8.9	8.8	8.9
m″-PyH	59.9	58.6	58.4	58.9	8.2	50.4	50.2	50.7
CH3*	-24	-42.0	-41.8	-42.2	2.6	-44.6	-44.4	-44.8

Table S8: Calculated orbital chemical shifts (in ppm) in the $[Mn(AcPyOx)_3(BPh)]^+$ complex with the different DFT functionals. The experimental chemical shifts in the diamagnetic $[Fe(AcPyOx)_3(BPh)]^+$ complex are given for comparison.

	PBE	PBE0	M06	M06-2X	CAM-B3LYP	B2PLYP	Exp
o-PhC	138.8	140.6	147.0	159.0	142.1	141.5	131.7
m-PhC	135.1	136.5	143.1	154.5	138.6	137.7	127.4
p-PhC	136.7	138.0	144.1	155.6	139.7	138.6	128.0
i-PhC	145.4	147.9	155.2	170.4	152.0	151.3	-
o′-PyC	151.2	155.0	164.8	173.2	158.0	158.4	153.0
m′-PyC	132.0	132.9	139.4	150.5	134.5	132.8	125.8
p-PyC	147.9	151.8	160.0	172.4	154.9	155.0	137.9
m″-PyC	129.5	131.3	137.2	147.8	133.1	131.9	124.5
o″-PyC	159.9	163.1	171.6	182.3	167.6	167.4	158.0
*C=N	157.4	160.8	171.2	180.1	163.5	164.8	160.6
*CH3	10.4	10.6	11.4	10.4	9.7	11.5	13.2
o-PhH	8.2	8.2	8.4	9.2	8.1	7.9	7.8
m-PhH	8.1	8.0	8.1	9.1	7.8	7.6	7.4
p-PhH	8.0	8.0	8.1	9.1	7.8	7.6	7.4
o′-PyH	8.8	8.9	9.0	9.9	8.9	8.7	7.1
m′-PyH	7.6	7.7	7.8	8.7	7.8	7.6	7.5
p-PyH	8.2	8.3	8.4	9.3	8.5	8.3	8.1
m″-PyH	7.8	7.9	8.0	8.9	8.0	7.8	7.9
CH3*	2.5	2.5	2.5	2.7	2.6	2.4	2.7

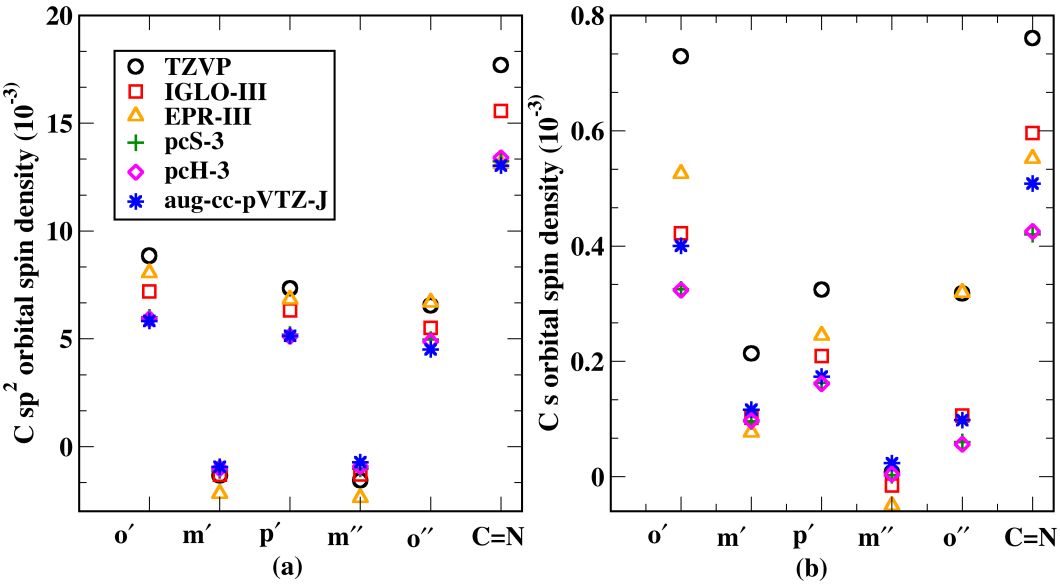

Figure S1: Löwdin ligand-atomic sp^2 hybrid orbital spin populations and their components in the s orbitals deduced for the C atoms for the different basis sets for the $[Mn(AcPyOx)_3(BPh)]^+$ complex.

Table S9: Calculated orbital chemical shifts (in ppm) in the $[Ni(AcPyOx)_3(BPh)]^+$ complex with the different DFT functionals. The experimental chemical shifts in the diamagnetic $[Fe(AcPyOx)_3(BPh)]^+$ complex are given for comparison.

	PBE	PBE0	M06	M06-2X	CAM-B3LYP	B2PLYP	Exp
o-PhC	137.8	139.7	136.7	157.1	142.2	141.1	131.7
m-PhC	135.1	136.3	134.2	153.9	138.9	137.5	127.4
p-PhC	136.9	138.0	135.6	155.4	140.3	138.8	128.0
i-PhC	144.7	147.0	144.3	167.8	151.6	150.5	-
o′-PyC	152.2	156.5	158.1	181.6	159.8	160.0	153.0
m′-PyC	131.3	132.4	130.4	149.7	134.9	132.9	125.8
p-PyC	146.2	150.9	149.6	172.2	154.8	154.9	137.9
m″-PyC	130.7	132.0	129.3	149.9	134.4	132.6	124.5
o″-PyC	161.6	164.7	163.6	187.5	169.1	168.4	158.0
*C=N	158.0	163.0	165.9	189.3	166.3	167.5	160.6
*CH3	12.4	12.0	10.9	13.8	11.3	12.5	13.2
o-PhH	7.9	7.9	7.9	8.3	7.8	7.6	7.8
m-PhH	7.7	7.7	7.7	8.5	7.7	7.4	7.4
p-PhH	7.8	7.7	7.7	8.7	7.7	7.5	7.4
o′-PyH	8.0	7.9	7.3	7.0	7.9	7.7	7.1
m′-PyH	7.6	7.6	7.5	8.4	7.6	7.4	7.5
p-PyH	8.3	8.4	8.3	9.6	8.5	8.4	8.1
m″-PyH	8.1	8.2	8.2	9.8	8.2	8.0	7.9
CH3*	2.6	2.6	2.5	3.1	2.6	2.5	2.7

Table S10: Calculated paramagnetic chemical shifts (in ppm) in the $[Mn(AcPyOx)_3(BPh)]^+$ complex according to VV approach where the hyperfine tensors were calculated with the different DFT functionals. The experimental paramagnetic chemical shifts are taken from Table S5.

	PBE	PBE0	M06	M06-2X	CAM-B3LYP	B2PLYP	Exp
o-PhC	-2.8	-2.2	-3.0	2.9	0.4	-2.0	13.7
m-PhC	5.3	4.3	1.7	2.8	3.3	5.5	3.9
p-PhC	-4.1	-4.0	-2.7	-2.5	-2.6	-5.1	-0.1
i-PhC	-30.1	-22.1	-49.5	-29.5	-18.9	-9.3	-
o′-PyC	1006.8	793.2	917.5	782.6	751.8	621.9	-
m′-PyC	618.7	388.6	482.1	367.2	413.8	253.5	510.1
p-PyC	279.4	231.5	124.8	244.0	182.8	222.7	253.7
m″-PyC	104.4	22.0	99.4	90.6	94.5	5.2	63.7
o″-PyC	-98.5	-189.6	-188.6	24.2	-176.6	-291.4	-
*C=N	405.0	344.4	400.9	815.7	463.6	611.6	646.4
*CH3	58.8	5.5	14.8	98.6	38.8	-76.0	-1.5
o-PhH	2.2	1.0	0.5	0.3	1.1	0.9	0.7
m-PhH	-0.5	-0.5	-0.7	-0.2	-0.4	-0.6	-0.1
p-PhH	1.5	0.8	1.2	0.4	0.6	0.8	0.1
o′-PyH	170.3	106.7	165.4	39.9	119.8	77.4	96.9
m′-PyH	56.3	42.5	37.5	28.0	41.3	38.5	39.5
p-PyH	-56.1	-43.2	-61.2	-29.7	-36.3	-40.0	-34.0
m″-PyH	69.6	49.3	47.3	38.3	49.2	41.1	39.1
CH3*	171.2	121.3	118.4	81.2	118.4	113.8	-

Table S11: Calculated paramagnetic chemical shifts (in ppm) in the $[Ni(AcPyOx)_3(BPh)]^+$ complex according to VV approach where the hyperfine tensors were calculated with the different DFT functionals. The experimental paramagnetic chemical shifts are taken from Table S5.

	PBE	PBE0	M06	M06-2X	CAM-B3LYP	B2PLYP	Exp
o-PhC	16.4	9.3	12.3	7.1	10.2	7.9	16.0
m-PhC	4.0	2.1	3.2	3.7	1.9	1.4	2.6
p-PhC	-0.7	-1.1	-1.2	-1.1	-0.7	-0.8	0.0
i-PhC	-82.2	-60.8	-77.8	-47.1	-57.5	-52.9	-
o′-PyC	-98.4	-204.1	-352.1	-184.3	-179.9	-260.7	-162.6
m′-PyC	687.4	461.7	493.5	363.9	437.5	287.6	418.4
p-PyC	-17.7	-20.9	3.8	-54.0	-14.6	-3.4	-21.6
m″-PyC	434.3	286.7	334.7	251.0	272.3	153.9	268.6
o″-PyC	-249.6	-236.4	-326.8	-114.6	-209.2	-90.6	-274.9
*C=N	372.1	-109.2	-82.2	-142.8	-122.6	-708.8	-106.6
*CH3	447.7	384.2	391.1	329.2	370.9	399.7	308.8
o-PhH	3.7	0.3	1.0	-1.6	0.5	-0.5	-0.4
m-PhH	-0.8	-0.7	-0.5	0.7	-0.6	-0.6	-0.8
p-PhH	0.2	-0.1	0.0	-0.2	-0.2	-0.2	-0.5
o′-PyH	244.5	147.9	201.9	115.3	143.3	97.5	130.2
m′-PyH	66.6	37.4	37.1	24.1	32.6	28.2	36.6
p-PyH	17.3	8.9	20.7	6.2	7.3	6.2	7.4
m″-PyH	85.8	50.4	53.1	36.8	46.0	39.3	52.0
CH3*	-36.2	-44.6	-52.3	-29.0	-49.8	-79.0	-26.7

Table S12: Mean absolute residuals (MAR) (in ppm) of the calculated ^{13}C and ^{1}H chemical shifts in the Mn and Ni $[M(AcPyOx)_3(BPh)]^+$ complexes for the different DFT functionals and the basis sets with respect to experimental chemical shifts reported in Table S5. The MAR of the calculated diamagnetic (Dia) and paramagnetic (Para) chemical shifts for each method are reported separately.

			Dia		Para	
	^{13}C	^{1}H	^{13}C	^{1}H	^{13}C	^{1}H
PBE	91	24	5.2	0.4	91	23
PBE0	40	5	6.7	0.4	41	5
M06	53	15	9.6	0.4	55	15
M06-2X	49	8	24.1	1.2	45	8
CAM-B3LYP	36	6	9.2	0.4	35	6
B2PLYP	91	9	8.5	0.3	96	9
TZVP	44	5	3.9	0.4	47	5
EPR-III	67	10	9.1	1.3	66	9
aug-cc-pVTZ-J	40	8	5.9	0.6	41	7
pcS-3	47	11	6.8	0.5	48	7
pcH-3	40	12	8.0	0.5	41	8

Table S13: Diamagnetic contribution (in ppm) to the orbital chemical shifts in the $[Ni(AcPyOx)_3(BPh)]^+$ complex with the different DFT functionals. Absolute values are given.

	PBE	PBE0	M06	M06-2X	CAM-B3LYP	B2PLYP
o-PhC	262.0	260.5	265.6	257.2	259.1	258.9
m-PhC	250.2	249.3	264.6	251.5	247.7	247.4
p-PhC	239.6	239.6	261.4	245.6	238.3	237.9
i-PhC	256.5	255.7	250.3	248.0	251.9	251.5
o′-PyC	263.1	262.0	269.0	260.2	260.8	260.7
m′-PyC	256.4	255.8	270.8	255.7	254.2	254.3
p-PyC	252.1	252.4	270.9	256.3	251.3	251.4
m″-PyC	262.9	261.8	276.2	261.9	260.4	259.8
o″-PyC	260.3	259.0	258.8	255.7	257.7	257.8
*C=N	259.3	259.0	261.2	261.3	258.5	258.5
*CH3	255.4	254.6	274.9	250.8	252.5	252.5
o-PhH	38.3	38.1	40.2	37.2	38.0	38.3
m-PhH	24.6	24.9	24.1	26.3	25.1	25.2
p-PhH	17.4	18.2	16.1	20.9	18.6	18.8
o′-PyH	42.5	41.9	43.7	40.2	41.3	41.5
m′-PyH	31.0	30.9	30.0	30.9	30.8	30.8
p-PyH	26.3	26.5	24.7	27.3	26.6	26.7
m″-PyH	31.6	31.7	32.5	32.1	31.9	32.1
CH3*	32.4	32.4	34.4	32.5	32.2	32.6

Table S14: Paramagnetic contribution (in ppm) to the orbital chemical shifts in the $[Ni(AcPyOx)_3(BPh)]^+$ complex with the different DFT functionals. Absolute values are given.

	PBE	PBE0	M06	M06-2X	CAM-B3LYP	B2PLYP
o-PhC	-218.9	-214.7	-235.1	-235.7	-217.6	-213.2
m-PhC	-204.3	-200.1	-230.9	-226.8	-202.9	-198.1
p-PhC	-195.5	-192.2	-229.0	-222.4	-194.9	-189.9
i-PhC	-220.3	-217.1	-227.5	-237.2	-219.8	-215.2
o′-PyC	-234.3	-233.1	-261.5	-263.2	-236.8	-233.9
m′-PyC	-206.8	-202.7	-233.0	-226.8	-205.5	-200.4
p-PyC	-217.4	-217.8	-253.2	-249.9	-222.4	-219.5
m″-PyC	-212.7	-208.4	-238.2	-233.2	-211.1	-205.6
o″-PyC	-241.0	-238.2	-256.6	-264.5	-243.1	-239.3
*C=N	-236.4	-236.5	-261.0	-272.0	-241.0	-239.2
*CH3	-86.9	-81.1	-111.9	-85.9	-80.1	-78.1
o-PhH	-14.6	-14.4	-16.2	-13.7	-14.1	-14.2
m-PhH	-0.7	-1.0	0.0	-3.0	-1.0	-0.9
p-PhH	6.5	5.7	8.0	2.3	5.4	5.4
o′-PyH	-18.9	-18.3	-19.6	-15.4	-17.5	-17.5
m′-PyH	-6.9	-6.9	-5.9	-7.5	-6.8	-6.6
p-PyH	-3.0	-3.3	-1.4	-5.1	-3.3	-3.4
m″-PyH	-8.1	-8.3	-9.0	-10.0	-8.4	-8.4
CH3*	-3.5	-3.4	-5.2	-3.8	-3.2	-3.4

Table S15: Calculated and experimental NMR chemical shifts (in ppm) in the $[Co(AcPyOx)_3(BPh)]^+$ complex. The orbital (Orb) and paramagnetic (Para) dipolar (Dip) and contact (Con) contributions (in ppm) to the calculated NMR chemical shifts are highlighted. The diamagnetic and contact contributions (in ppm) were calculated at unrestricted DFT ZORA-PBE0/IGLO-III level of theory. The dipolar contributions were calculated considering the semi-classical point-dipolar (PD) equation (eq. S4) or based on the two QC methods, namely the unrestricted DFT ZORA-PBE0 (PBE0) and SO-CASSCF (CAS) based hyperfine tensors according to VV approach.

	Orb	Para				Cal =			Exp
		Dip			Con	Orb+Dip+Con			
		PD	PBE0	CAS		PD	PBE0	CAS	
o-PhC	140.7	94.0	54.4	98.2	7.1	241.8	202.2	246.0	208.6
m-PhC	136.5	50.0	27.2	52.4	4.4	190.9	168.1	193.3	164.7
p-PhC	138.0	40.9	24.3	42.9	-1.8	177.1	160.5	179.1	155.4
i-PhC	148.9	166.0	89.1	172.5	-74.2	240.7	163.8	247.2	
o′-PyC	159.7	200.7	197.9	228.8	-175.4	185.0	182.2	213.1	263.9
m′-PyC	131.1	42.0	9.4	44.9	526.6	699.7	667.1	702.6	554.9
p-PyC	150.9	-20.3	4.0	-20.2	2.7	133.3	157.6	133.4	146.7
m″-PyC	131.4	-86.6	-58.2	-89.4	271.7	316.5	344.9	313.7	318.3
o″-PyC	163.6	-302.0	-76.0	-314.0	-617.5	-755.9	-529.9	-767.9	-476.5
*C=N	162.3	-235.2	-79.9	-248.1	-73.8	-146.7	8.6	-159.6	97.7
*CH3	10.8	-50.7	-26.2	-52.3	256.3	216.4	240.9	214.8	189.4
o-PhH	9.1	86.4	50.9	90.5	1.3	96.8	61.3	100.9	67.9
m-PhH	8.2	34.2	19.7	35.8	-0.1	42.3	27.8	43.9	29.9
p-PhH	8.4	27.3	15.8	28.6	0.6	36.3	24.8	37.6	25.7
o′-PyH	12.1	362.4	194.3	377.7	172.7	547.2	379.1	562.5	396.2
m′-PyH	8.2	46.3	28.4	49.8	41.1	95.6	77.7	99.1	80.1
p-PyH	8.3	-12.0	-5.0	-12.6	-1.8	-5.5	1.5	-6.1	15.1
m″-PyH	7.5	-63.3	-33.9	-66.6	47.1	-8.7	20.7	-12.0	-2.5
CH3*	2.3	-29.0	-17.3	-30.5	17.1	-9.6	2.1	-11.1	2.4

Table S16: Calculated NMR chemical shifts (in ppm) in the $[Co(AcPyOx)_3(BPh)]^+$ complex according to the mPV and BB approaches. The orbital (Orb) and paramagnetic dipolar (Dip) and contact (Con) contributions (in ppm) to calculated NMR chemical shifts are reported. Unrestricted DFT ZORA-PBE0/IGLO-III based hyperfine tensors were used to calculate the paramagnetic chemical shifts.

		Para				Cal =		
	Orb	mPV		BB		Orb+Dip+Con		Exp
		Dip	Con	Dip	Con	mPV	BB	
o-PhC	140.7	62.8	6.8	60.2	7.4	210.3	208.3	208.6
m-PhC	136.5	31.4	4.4	30.1	4.7	172.3	171.3	164.7
p-PhC	138.0	28.0	-1.8	26.8	-1.9	164.2	162.9	155.4
i-PhC	148.9	102.7	-70.0	98.5	-77.0	181.6	170.4	
6-PyC	159.7	226.6	-171.3	218.7	-184.1	215.0	194.3	263.9
5-PyC	131.1	12.7	501.4	11.1	548.0	645.2	690.2	554.9
4-PyC	150.9	4.4	0.8	4.9	2.0	156.1	157.8	146.7
3-PyC	131.4	-68.0	260.0	-64.7	283.3	323.4	350.0	318.3
2-PyC	163.6	-89.1	-594.6	-84.4	-645.1	-520.1	-565.9	-476.5
C=N	162.3	-94.7	-68.8	-88.2	-76.6	-1.2	-2.5	97.7
*CH3	10.8	-30.6	243.3	-29.1	266.5	223.5	248.2	189.4
o-PhH	9.1	58.7	1.3	56.3	1.4	69.1	66.8	67.9
m-PhH	8.2	22.7	-0.1	21.8	-0.1	30.8	29.9	29.9
p-PhH	8.4	18.2	0.5	17.5	0.6	27.1	26.5	25.7
6-PyH	12.1	224.0	166.1	214.7	180.3	402.2	407.1	396.2
5-PyH	8.2	32.9	38.9	31.4	42.7	80.0	82.3	80.1
4-PyH	8.3	-5.7	-2.0	-5.5	-1.9	0.6	0.9	15.1
3-PyH	7.5	-39.1	44.5	-37.5	49.0	12.9	19.0	-2.5
CH3*	2.3	-20.0	16.3	-19.2	17.8	-1.4	0.9	2.4

Table S17: The three principal g-values and the $\langle \mathbf{S} \cdot \mathbf{S} \rangle$ ($\times \mu_0 \mu_B^2 N_A$) tensor components (in 10^{-8} $m^3 mol^{-1}$) (at 298 K) of the 2 KDs (modeled with $\tilde{S} = 3/2$) and 3 KDs (modeled with $\tilde{S} = 5/2$).

	$\tilde{S}$	g_1, g_2, g_3	$\langle \mathbf{S} \cdot \mathbf{S} \rangle$
2 KDs	3/2	1.72, 1.76, 3.25	1.07, 1.10, 2.69
3 KDs	5/2	1.40, 1.40, 1.75	1.41, 1.43, 2.55

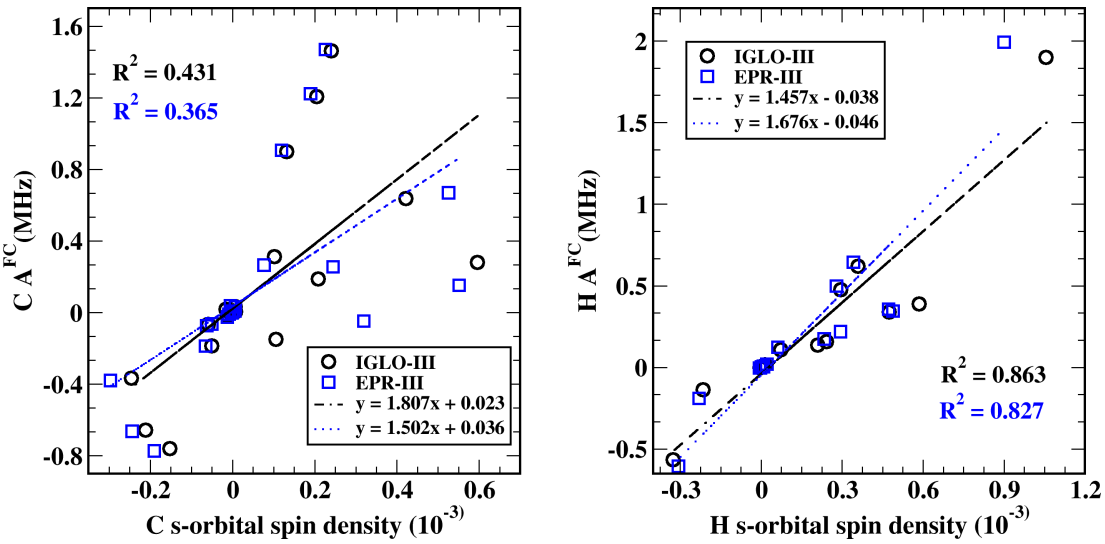

Figure S2: Correlation plots of the Fermi-contact Hyperfine coupling constants A^{FC} vs the s-orbitals' spin populations ρ_s^s for the ligand C and H atoms calculated at unrestricted DFT ZORA-PBE0 level of theory. The slopes ($\times 10^3$) can be compared to the hyperfine coupling constant G (in MHz) with an unpaired electron in the atomic valence s-orbital (ns): for H 1s orbital, experimental $G = 1420$ MHz and for C 2s orbital, theoretical $G = 3760$ MHz from Ref.[10], 5520 MHz from ZORA-PBE0/EPR-III and 5516 MHz from ZORA-PBE0/IGLO-III.

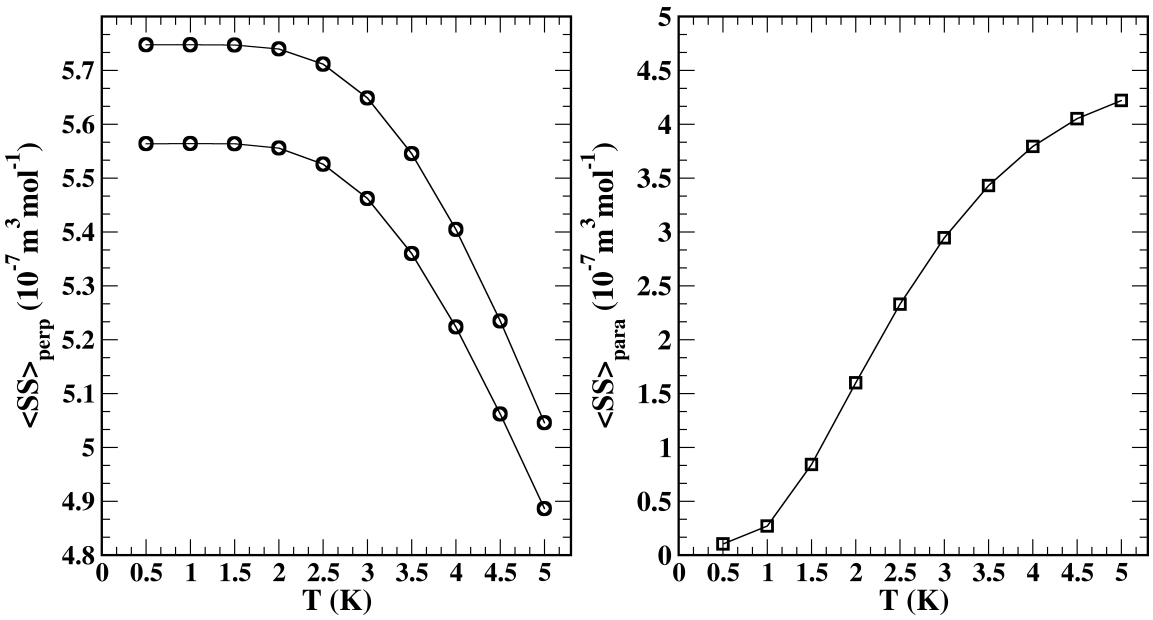

Figure S3: Temperature dependence of the perpendicular (perp) and parallel (para) components of the diagonal $\langle \mathbf{S} \cdot \mathbf{S} \rangle$ ($\times \mu_0 \mu_B^2 N_A$) tensor in the $[\mathrm{Ni(AcPyOx)_3(BPh)}]^+$ complex evaluated according to eq. 11 in the three lowest energy states and by neglecting the orbital Zeeman contribution to the energy Hamiltonian matrix of $\hat{H}\,(\hat{m}_i; B_0)$ operator. The calculated very-low temperature behavior of the perpendicular and parallel components directly from the SO-CASPT2 space are in accordance with the reported behavior by Soncini and Van den Heuvel for a triplet model space ($\tilde{S} = 1$) with $D > 0$ (D=7.5 cm^{-1}) in Ref.[11] (ZFS parts of eq. 8).

References

(1) Kutzelnigg, W. Origin and meaning of the Fermi contact interaction. *Theor. Chim. Acta* **1988**, *73*, 173–200.

(2) van Lenthe, E.; Van Der Avoird, A.; Wormer, P. E. Density functional calculations of molecular hyperfine interactions in the zero order regular approximation for relativistic effects. *J. Chem. Phys.* **1998**, *108*, 4783–4796.

(3) Sharkas, K.; Pritchard, B.; Autschbach, J. Effects from Spin–Orbit Coupling on Electron–Nucleus Hyperfine Coupling Calculated at the Restricted Active Space Level for Kramers Doublets. *J. Chem. Theory Comput.* **2015**, *11*, 538–549.

(4) Autschbach, J.; Patchkovskii, S.; Pritchard, B. Calculation of hyperfine tensors and paramagnetic NMR shifts using the relativistic zeroth-order regular approximation and density functional theory. *J. Chem. Theory Comput.* **2011**, *7*, 2175–2188.

(5) Malkin, I.; Malkina, O. L.; Malkin, V. G.; Kaupp, M. Scalar relativistic calculations of hyperfine coupling tensors using the Douglas–Kroll–Hess method. *Chem. Phys. Lett.* **2004**, *396*, 268–276.

(6) Autschbach, J. Relativistic Effects on Electron-Nucleus Hyperfine Coupling Studied with an Exact 2-Component (X2C) Hamiltonian. *J. Chem. Theory Comput.* **2017**, *13*, 710–718.

(7) Sandhoefer, B.; Kossmann, S.; Neese, F. Derivation and assessment of relativistic hyperfine-coupling tensors on the basis of orbital-optimized second-order Møller–Plesset perturbation theory and the second-order Douglas–Kroll–Hess transformation. *J. Chem. Phys.* **2013**, *138*, 104102.

(8) Pavlov, A. A.; Nehrkorn, J.; Pankratova, Y. A.; Ozerov, M.; Mikhalyova, E. A.; Polezhaev, A. V.; Nelyubina, Y. V.; Novikov, V. V. Detailed electronic structure of

a high-spin cobalt (II) complex determined from NMR and THz-EPR spectroscopy. *Phys. Chem. Chem. Phys.* **2019**, *21*, 8201–8204.

(9) Pavlov, A. A.; Savkina, S. A.; Belov, A. S.; Nelyubina, Y. V.; Efimov, N. N.; Voloshin, Y. Z.; Novikov, V. V. Trigonal prismatic tris-pyridineoximate transition metal complexes: A cobalt (II) compound with high magnetic anisotropy. *Inorg. Chem.* **2017**, *56*, 6943–6951.

(10) Hurd, C.; Coodin, P. Atomic parameters for the interpretation of ESR and diamagnetic susceptibility data. *J. Phys. Chem. Solids* **1967**, *28*, 523–525.

(11) Soncini, A.; Van den Heuvel, W. Communication: Paramagnetic NMR chemical shift in a spin state subject to zero-field splitting. *J Chem Phys* **2013**, *138*, 021103.